Pham, T. and Hadi, M. and Tran, T. 2015. Maximum usable strain of FRP-confined concrete. Construction and Building Materials. 83: pp. 119-127.

ABSTRACT

This study investigates the progressive failure of FRP-confined concrete. Ten FRP-confined concrete specimens were divided into two groups with different jacket stiffness. One specimen in each group was tested until failure while the others were loaded to target strains and then unloaded in order to monitor the residual strength of the concrete cores. At 1% axial strain of FRP-confined concrete, the residual strength of the concrete cores were reduced more than 56% compared to the reference specimens. Experimental results have shown that the maximum usable strain of 1% is un-conservative for FRP-confined concrete. A model is proposed to estimate the residual strength of concrete cores. Predictions from the proposed model fit the experimental results well. In addition, a new procedure is proposed to determine the maximum usable strain of FRP-confined concrete based on the maximum usable strain of unconfined concrete.

Keywords: Axial strain; Failure mechanisms; Maximum usable strain.

Maximum Usable Strain of FRP-Confined Concrete

Thong M. Pham[1], Muhammad N.S. Hadi[2] and Tung M. Tran[3]

[1]Postdoctoral Research Associate, School of Civil and Mechanical Engineering, Curtin University, Kent Street, Bentley, WA 6102, Australia; Formerly, PhD Scholar, School of Civil, Mining and Environmental Engineering, University of Wollongong, Wollongong, NSW 2522, Australia. Email: thong.pham@curtin.edu.au

[2]Associate Professor, School of Civil, Mining and Environmental Engineering, University of Wollongong, NSW 2522, Australia (corresponding author). Email: mhadi@uow.edu.au

[3]Lecturer, Department of Civil Engineering, Ton Duc Thang University, Ho Chi Minh, Vietnam, currently a PhD Scholar at the School of Civil, Mining and Environmental Engineering, University of Wollongong, Wollongong NSW 2522, Australia. E-mail: tmt954@uowmail.edu.au

1. Introduction

Fibre Reinforced Polymer (FRP) has been commonly used to strengthen existing reinforced concrete (RC) columns in recent years [1-3]. In such cases, FRP is a confining material for concrete in which the confinement effect leads to increase the strength and ductility of columns. In early experimental studies of FRP retrofitted RC columns, the axial capacities of strengthened columns increased significantly as compared to reference columns. The database collected by Lee and Hegemier [4] showed that FRP-confined concrete cylinders have maximum compressive strain ranging from 0.6% to 4.2% while Teng et al. [5] showed that the maximum compressive strain of specimens varied from 0.8% to 3.7%. Pham and Hadi [6] collected a database of 167 FRP-confined concrete columns where the maximum compressive strain of the columns ranged between 0.5% and 4%. Ilki et al. [7] conducted experiments on FRP-confined circular and rectangular RC columns. Results from this study had shown that the maximum compressive strain of FRP-confined concrete ranged from 1.3% to 8.6%. The maximum compressive strain up to 9.66% was recorded from the experimental study carried out by Dai et al. [8] on RC columns confined with large rupture strain and the maximum compressive strain up to 10.4 % was reached in Ilki et al.'s study [9] on FRP confined low strength concrete members. From the literature, it can be seen that the maximum compressive

strain of FRP-confined concrete varies in a broad range and no study has shown a maximum usable strain of confined concrete [10-14]. Meanwhile, ACI-440.2R [15] and The Concrete Society [16] provided maximum usable strain of 1% for FRP-confined concrete to prevent excessive cracking and the resulting loss of concrete integrity.

In addition, ACI-440.2R [15] defines the maximum usable strain of unconfined concrete. However, there is no definition for maximum usable strain of confined concrete in ACI-440.2R [15]. As mentioned above, experimental studies have shown that the maximum compressive strain of FRP-confined concrete varies in a wide range from 0.5% to 10.4%. However, these studies did not investigate the integrity of the concrete during testing. No study has investigated the precise nature of the progressive failure mechanisms occurring during experimental tests. In other words, a limit of 1% for maximum compressive strain for confined concrete recommended by the two guidelines [15, 16] seems small as compared to the experimental results. Therefore, determining the nature of the progressive failure mechanisms and the maximum usable strain of FRP-confined concrete is essentially necessary. This study conducted experimental tests to investigate the progressive failure mechanisms of FRP-confined concrete at many stages of testing.

2. Axial Strain of Concrete

A typical stress-strain relation of unconfined concrete is shown in Fig. 1. The stress-strain curve rises to a maximum stress, reached at a strain between 0.15% and 0.3%, followed by a descending branch [17]. The length of the descending branch of the curve is strongly affected by the test conditions. Usually, an axially loaded concrete cylinder fails at the maximum stress. In such cases, the stress-strain curve suddenly drops from the maximum stress. On the other hand, if a structural member is loaded in compression due to bending (or bending plus axial load), the descending branch might exist as shown in the solid line after the maximum

stress in Fig. 1 [17]. This study deals with pure compression tests so that the failure of unconfined concrete is approximately determined at the maximum stress stage that has a corresponding strain between 0.15% and 0.3%.

In addition, stress-strain relations of FRP-confined concrete are also presented in Fig. 1. Based on the confinement ratio, the stress-strain relation of FRP-confined concrete may belong to an ascending branch or a descending branch. Specimens with low stiffness confinement yield a descending branch stress-strain curve as described by The Concrete Society [16]. The axial stress of these specimens reaches the maximum stress before FRP rupture. Conversely, the axial stress of specimens that have stiff confinement reaches the maximum stress at the FRP rupture. Therefore, the maximum compressive strain of FRP-confined concrete is the measured axial strain of specimens as FRP ruptures due to tension forces in hoop direction. There is a consensus that the core of FRP-confined concrete can resist the applied load until FRP ruptured without any investigation about the progressive failure mechanisms. No study about confined concrete has verified the integrity of the concrete core during testing. As a result, the failure indicator of FRP-confined concrete is controlled by the failure of the FRP jacket. This failure determination complies with the failure definition of concrete confined by helical steel reinforcement [18]. Mander et al. [18] defined that the maximum axial strain of confined concrete was reached when the first lateral reinforcement fractures. However, this study focuses on the failure of the concrete cores not the FRP.

3. Experimental Program

3.1. Design of Experiments

A total of thirteen standard concrete cylinders were cast and tested at the High Bay laboratory of the University of Wollongong. The dimensions of the specimens were 150 mm by 300 mm

and the design compressive strength of concrete was 50 MPa. The specimens were classified into three groups, namely, the reference group (R), two layers group (C2) and three layers group (C3). Details of the specimens are presented in Table 1. The notation of the specimens consists of two parts: the first part is “R”, “C2”, and “C3” stating the name of the groups. The second part indicates the target strains of the specimens at which the loading was stopped. For example, Specimen C2-1.9 indicates the specimen which was wrapped with two layers of FRP and loaded up to 1.9% axial strain.

After 28 days, each specimen was symmetrically bonded at midheight with two 60 mm strain gages in the vertical direction and two 60 mm strain gages in the horizontal direction. The specimens on group C2 and C3 were then fully wrapped with carbon FRP (CFRP) layers using a wet lay-up method. The adhesive was a mixture of epoxy resin and hardener at 5:1 ratio and the amount of FRP layers in the specimens is described in Table 1. For each specimen, four CFRP rings of 75 mm width were applied in the hoop direction to ensure that the whole specimen (300 mm length) was wrapped with layers of CFRP. Before the first layer of CFRP was attached, the adhesive was spread onto the surface of the specimen and CFRP was attached onto the surface. After the first layer, the adhesive was spread onto the surface of the first layer of CFRP and the second layer was continuously bonded. The third layer of CFRP was applied in a similar manner, ensuring that an overlap of 100 mm was maintained.

In order to measure the lateral strain of the specimens, four strain gages were symmetrically bonded in the hoop direction of the jacket. Details of the positions of the strain gages are shown in Fig 2. During the testing, the FRP jacket would cause confining pressure perpendicularly to the concrete surface and thus the strain gages on the concrete surface. This confining pressure could affect the readings from these strain gages.

3.2. Instrumentation

The Denison 5000 KN testing machine was used for testing all the specimens. The columns were capped with high strength plaster at both ends to ensure full contact between the loading heads and the column. Calibration was then performed to ensure that the columns were placed at the center of the testing machine. The tests were conducted as displacement controlled with a rate of 0.5 mm/min. All the strain gages were connected with a data logger and simultaneously saved in a control computer.

Furthermore, the longitudinal compressometer as shown in Fig. 3 was used to measure the axial strain of the specimens and then these readings were compared to those from the strain gages. A linear variable differential transformer (LVDT) was mounted on the upper ring and the tip of the LVDT rests on an anvil. The readability, the accuracy, and the repeatability of the LVDT comply with the Australian standard [19]. This LVDT was also connected to the data logger and the readings were saved in the control computer.

3.3. Testing Scheme

The axial stress and strain of the specimens were predicted using the study by Jiang and Teng [20]. Since the maximum strain of the specimens was determined, each specimen was tested to reach the single target axial strain as described in Table 1. The first specimen in that group was tested until the axial strain reached 0.6% that was the average value between 0.2% and 1%. The value of 0.2% was adopted from the widely accepted maximum axial strain of unconfined concrete while the value of 1% was proposed by ACI-440.2R [15] for the maximum usable strain of FRP-confined concrete. The other specimens were tested to a target axial strain that range equally from 1% to the maximum axial strain of the group. After the tested specimens were loaded to the target strains, these specimens were unloaded and unwrapped in order to investigate any cracks which may have developed during the testing.

The concrete cores of these specimens were then tested again under compression load to examine the integrity of the concrete and their residual strengths.

4. Experimental Results

4.1. Preliminary tests

The actual compressive strength of unconfined concrete calculated from three reference Specimens (R-1, R-2, and R-3) was 52.08 MPa. The axial strain of unconfined concrete at the maximum load was 0.24%. CFRP used in this study was 75 mm in width with a unidirectional fibre density of 340 g/m^2. Five CFRP coupons were made according to ASTM D7565 [21] and tested to determine their mechanical properties. The coupons were made of three layers of FRP and had a nominal thickness of 1.45 mm. The average width of the coupons was 24.86 mm and the average maximum tensile force per unit width was 2037 N/mm. The strain at the maximum tensile force and the average elastic modulus were 0.0165 mm/mm and 123 kN/mm, respectively.

The axial strain of specimens was measured by both strain gages attached on the surface of concrete and LVDT mounted on the compressometer. Two readings were almost identical at early stages of the testing. However, the strain gages on the concrete failed at a strain about 0.6 -0.7%, which may have resulted from the high confining pressure of the jacket. As a result, the experimental axial strains reported in this study are the readings from the LVDT.

4.2. Failure modes and stress-strain Relation

Specimens C2-1.9 and C3-2.4 were tested until fail. These specimens failed by FRP rupture, resulting in loud explosive sounds. The rupture strain of FRP is the average values from three strain gages outside the overlap zone. The other specimens were loaded to the target strains and then their jackets were peeled off to investigate the damage level of the column cores.

Specimens with high axial strain (C2-1.2, C2-1.4, C3-1.4, and C3-1.7) had wide and long cracks on the cores as shown in Fig. 4. These cracks were formed vertically and they cut throughout the core from the top to the bottom. These specimens were damaged and could not be used as the section of the cores was significantly reduced. Cores of the remaining specimens were loaded again until failure to examine the residual compressive strength and the results are shown in Table 2. The residual strength of these specimens was less than 20% as compared to the reference specimens. Meanwhile, specimens with lower axial strain (C2-0.6, C2-1.0, C3-0.6, and C3-1.0) had less serious cracks and the cores still kept the cylindrical shape as shown in Fig. 5. These cracks formed locally and they had small width and short length. The residual strength of these specimens ranged from 40% to 60% as compared to the reference specimens (Table 2).

4.3. Residual Strength of the Cores

It is obvious that FRP prevents the cores from expanding under the applied loads. At the same value of axial strain, the lateral strain of specimens in Group C3 is lower than that of specimens in Group C2. Thus the residual strength of specimens in Group C3 is expected to be higher than that of the corresponding specimens in Group C2. Fig. 6 shows the residual strengths of Group C2 and Group C3. These experimental results confirm that with a similar axial strain the core of specimens that were wrapped with a thicker jacket will have higher residual strength as compared to the one wrapped with a thinner jacket. Thus it can be seen that the damage level of the cores is due to both the axial strain and the lateral strain, which is controlled by the stiffness of the jacket.

From the experimental results presented in Figs. 7-8, it can be seen that the residual strengths of the cores had values very close to the ordinate of the intersection between the unload curve and the unconfined concrete curve. These values are summarized in Table 2. Thus it is

assumed that the residual strength of the column cores is equal to the ordinate of the intersection between the unload curve and the unconfined concrete curve.

5. Theoretical Verification

5.1. Behavior of FRP-confined Concrete under Cyclic Load

Theoretical models about behavior of FRP-confined concrete under cyclic loads are studied and summarized to simulate the experimental results [22, 23]. The loading scheme of this study is illustrated in Fig. 9. FRP-confined concrete specimens were tested to Point *a*, that has the unloading strain (ε_{un}) and the unloading stress (σ_{un}), and then unloaded until Point *c*. Point *c* is determined by the reloading strain (ε_{re}) and the reloading stress (σ_{re}) that is equal to zero in this study. When Point *c* lies on the horizontal axis, the loading strain (ε_{re}) is equal to the plastic strain (ε_{pl}) (or permanent strain). During the unloading process, the unloading curve intersects the stress-strain curve of unconfined concrete at Point *b* that has the intersect strain (ε_{in}) and the intersect stress (σ_{in}).

The loading curve in Fig. 9 is the envelop curve in the study by Lam and Teng [22]. The model proposed by Lam and Teng [24] was adopted by Lam and Teng [22] to predict the envelop curve. However, this model did not yield good results as compared to the experimental results in this paper. Thus, the envelop curve (loading path) is estimated by the model proposed by Jiang and Teng [20], which is summarized in the section below. Meanwhile, the unloading path was calculated as follows [22]:

$$\sigma_c = a\varepsilon_c^{\eta} + b\varepsilon_c + c \tag{1}$$

$$a = \frac{\sigma_{un} - E_{un,0}\left(\varepsilon_{un} - \varepsilon_{pl}\right)}{\varepsilon_{un}^{\eta} - \varepsilon_{pl}^{\eta} - \eta\varepsilon_{pl}^{\eta-1}\left(\varepsilon_{un} - \varepsilon_{pl}\right)} \tag{2}$$

$$b = E_{un,0} - \eta\varepsilon_{pl}^{\eta-1}a \tag{3}$$

$$c = -a\varepsilon_{pl}^{\eta} - b\varepsilon_{pl} \tag{4}$$

$$\varepsilon_{pl} = \begin{cases} 0, & 0 < \varepsilon_{un} \le 0.001 \\ \left[1.4\left(0.87 - 0.004\, f_{co}^{'}\right) - 0.64\right]\left(\varepsilon_{un} - 0.001\right), & 0.001 < \varepsilon_{un} < 0.0035 \\ \left(0.87 - 0.004\, f_{co}^{'}\right)\varepsilon_{un} - 0.0016, & 0.0035 \le \varepsilon_{un} < \varepsilon_{cc} \end{cases} \tag{5}$$

where η is an exponent and $E_{un,0}$ is the slope of the unloading path at zero stress. The shape of an unloading path is controlled by the two parameters: η and $E_{un,0}$ that are calculated as follows [22]:

$$\eta = 350\varepsilon_{un} + 3 \tag{6}$$

$$E_{un,0} = min\left\{\frac{0.5\, f_{co}^{'}}{\varepsilon_{un}}; \frac{\sigma_{un}}{\varepsilon_{un} - \varepsilon_{pl}}\right\} \tag{7}$$

In addition, the stress-strain curve of unconfined concrete is predicted using the equations proposed by Sargin et al. [25] as follows:

$$\frac{\sigma_c}{\sigma_{co}} = \frac{A\frac{\varepsilon_c}{\varepsilon_{co}} + (D-1)\left(\frac{\varepsilon_c}{\varepsilon_{co}}\right)^2}{1 + (A-2)\frac{\varepsilon_c}{\varepsilon_{co}} + D\left(\frac{\varepsilon_c}{\varepsilon_{co}}\right)^2} \tag{8}$$

$$A = \frac{E_0}{E_c} \tag{9}$$

$$E_c = \frac{f_{co}^{'}}{\varepsilon_{co}} \tag{10}$$

where E_0 is the Young's modulus of elasticity (E_0 = 4730 $\sqrt{f_{co}^{'}}$, MPa), E_c is the secant modulus of elasticity at the peak, and D = 1 is the parameter which primarily governs the

descending part of the stress-strain curve. The reloading path is predicted by the same equations proposed Sargin et al. [25] with the exception of replacing the Young's modulus of elasticity (E_0) by the reloading stiffness (E_{re}), which is discussed in the section below. It is noted that the residual strength of the column core (Point *d*) is assumed to be equal to the ordinate of Point *b* in Fig. 9.

5.2. Envelop Curve and Reloading Stiffness

The model for FRP-confined concrete proposed by Jiang and Teng [20] was adopted to predict the envelop curve of the stress-strain curve. In that model, the axial stress and the axial strain of FRP-confined concrete at a given lateral strain are the same as those of the same concrete actively confined with a constant confining pressure equal to that provided by the FRP jacket. Fig. 10 illustrates the concept of this incremental approach. The stress-strain curve of FRP-confined concrete is obtained as presented by Jiang and Teng [20]:

1) For a given axial strain, find the corresponding lateral strain according to the lateral-to-axial strain relationship;

2) Based on force equilibrium and radial displacement compatibility between the concrete core and the FRP jacket, calculate the corresponding lateral confining pressure provided by the FRP jacket;

3) Use the axial strain and the confining pressure obtained from Steps (1) and (2) in conjunction with an active-confinement base model to evaluate the corresponding axial stress, leading to the identification of one point on the stress-strain curve of FRP-confined concrete;

4) Repeat the above steps to generate the entire stress–strain curve.

The following equations were adopted in the procedure above [20]:

$$\sigma_l = \frac{2E_f t\varepsilon_l}{d} \tag{11}$$

$$\frac{\varepsilon_c}{\varepsilon_{co}} = 0.85\left(1+8\frac{\varepsilon_l}{f_{co}^{'}}\right)\left\{\left[1+0.75\left(\frac{-\varepsilon_l}{\varepsilon_{co}}\right)\right]^{0.7} - e^{-7\left(\frac{-\varepsilon_l}{\varepsilon_{co}}\right)}\right\} \tag{12}$$

$$f_{cc}^{'*} = f_{co}^{'} + 3.5f_l \tag{13}$$

$$\frac{\varepsilon_{cc}^{*}}{\varepsilon_{co}} = 1+17.5\frac{\varepsilon_l}{f_{co}^{'}} \tag{14}$$

$$\frac{\varepsilon_c}{f_{cc}^{'*}} = \frac{r\frac{\varepsilon_c}{\varepsilon_{cc}^{*}}}{r-1+\left(\frac{\varepsilon_c}{\varepsilon_{cc}^{*}}\right)^r} \tag{15}$$

$$r = \frac{E_0}{E_0 - \frac{f_{cc}^{'*}}{\varepsilon_{cc}^{*}}} \tag{16}$$

where ε_l is the lateral strain, E_f is the elastic modulus of FRP, t is the thickness of FRP, d is the diameter of specimens, $f_{cc}{}^{'*}$ is the peak stress of concrete under a specific constant confining pressure f_l, $\varepsilon_{cc}{}^{*}$ is the axial strain at $f_{cc}{}^{'*}$, and r is the constant defined by Eq. 16**Error! Bookmark not defined.**.

The reloading stiffness E_{re} presented in the study by Lam and Teng [22] is shown in Fig. 11. The reloading stiffness is the slope of Line *cd* that is estimated as follows:

$$E_{re} = \frac{\sigma_{new}}{\varepsilon_{un} - \varepsilon_{pl}} \tag{17}$$

$$\phi = \frac{\sigma_{new}}{\sigma_{un}} \tag{18}$$

where ϕ is the stress deterioration ratio for the unloading/reloading cycle and σ_{new} is the new stress at the reference strain.

$$\phi = \begin{cases} 1, & 0 < \varepsilon_{un} \le 0.001 \\ 1 - 80(\varepsilon_{un} - 0.001), & 0.001 < \varepsilon_{un} < 0.002 \\ 0.92, & 0.002 \le \varepsilon_{un} < \varepsilon_{cc} \end{cases} \quad (19)$$

It is widely accepted that the confining effect of FRP is ignored as FRP-confined concrete is compressed at a stress level lower than the peak stress of unconfined concrete. Thus it is assumed that the Young's modulus of elasticity of the FRP-confined concrete and the column core is the same. In this study, the specimens were unloaded and the FRP jacket was peeled off before reloading to the peak stress of the column cores. The reloading stiffness of the column cores now is estimated based on the equations above, which are used for reloading FRP-confined concrete.

5.3. Comparison with Experimental Results

The procedure presented above is used to predict the residual strength of a column core. The experimental results and theoretical calculations of specimens in Group C3 are presented in Fig. 12. The theoretical calculations fit the experimental results well. Thus at a given axial strain of FRP-confined concrete, the residual strength of the column core can be estimated.

6. Maximum Usable Strain

The progressive failure mechanisms of FRP-confined concrete are not due to the FRP failing progressively but rather due to the concrete failing progressively [26]. In addition, Priestley et al. [27] recommended that the lateral strain of FRP-confined concrete columns should be limited to the value of 0.4% to prevent the degradation of aggregate interlock action, which is essential to the concrete shear resisting mechanism. Based on the experimental observations and the arguments above, this study recommends that the maximum usable strain of confined concrete should be controlled by the maximum usable strain of the concrete cores. It is worth mentioning that at the maximum usable strain FRP-confined RC concrete specimens must

maintain the bond between internal reinforcement and the concrete core and the aggregate interlock.

The specimens of Group C3 could resist axial loads until the axial strain of 2.64% was reached. Specimen C3-0.6 was loaded to reach the axial strain at 0.66% and then reloaded. However, the residual strength of this specimen reduced significantly by 42%, which may led to considerable decrease of the bonding between internal reinforcements and concrete as well as the aggregate interlock in RC concrete. This axial strain is much smaller than 1% as proposed by ACI 440.2R [15]. Therefore, the maximum usable strain of FRP-confined concrete should be controlled by the maximum usable strain of the concrete core.

However, the maximum usable strain of the concrete core in FRP-confined concrete has not been investigated. The maximum usable strain of unconfined concrete ($\varepsilon_{lim,\,u}$) proposed by ACI 318 [28] was adopted. ACI 318 [28] recommended that the maximum usable strain of unconfined concrete is 0.3%, which is equal to σ_{in} in Fig. 9. Given a stress-strain curve of unconfined concrete, Point *b* in Fig. 9 can be determined (*b* (0.3, 50)). Next, the maximum usable strain at Point *a* is also determined by iterative processes (*a* (0.32, 57)) for specimens of Group C3). Fig. 13 describes a flow chart to determine the maximum usable strain of FRP-confined concrete ($\varepsilon_{lim,\,u}$). Therefore, the maximum usable strain of FRP-confined concrete (ε_{lim}) given the properties of materials can be estimated if the maximum usable strain of unconfined concrete ($\varepsilon_{lim,\,u}$) is proposed. It is necessary to investigate the maximum usable strain of the concrete core in FRP-confined concrete.

7. Conclusions

This study investigated the progressive failure of FRP-confined concrete based on the failure of the concrete cores. The residual strengths of the concrete cores were determined

experimentally and theoretically at many axial strain levels. The findings presented in this paper are summarized as follows:

1. The residual strengths of the concrete cores were reduced more than 56% at the axial strain 1% of FRP-confined concrete.

2. A model was proposed to estimate the residual strength of the concrete cores of a FRP-confined concrete column at a certain axial strain.

3. The maximum usable strain of FRP-confined concrete is much smaller than the value of 1% proposed by ACI 440-2R [15].

Finally, the experimental results show that the maximum usable strain of FRP-confined concrete should be determined from that of unconfined concrete. The predictions of the proposed model fit the experimental results very well.

Acknowledgement

The first and third authors would like to acknowledge the Vietnamese Government and the University of Wollongong for the support of their full PhD scholarships. The authors thank Mr. Guan Lin, Ph.D. candidate at the Hong Kong Polytechnic University, for his useful comments.

References

[1] Pham TM, Doan LV, Hadi MNS. Strengthening square reinforced concrete columns by circularisation and FRP confinement. Constr Build Mater. 2013;49(0):490-9.

[2] Hadi MNS, Pham TM, Lei X. New Method of Strengthening Reinforced Concrete Square Columns by Circularizing and Wrapping with Fiber-Reinforced Polymer or Steel Straps. J Compos Constr. 2013;17(2):229-38.

[3] Hadi MNS, Widiarsa IBR. Axial and Flexural Performance of Square RC Columns Wrapped with CFRP under Eccentric Loading. J Compos Constr. 2012;16(6):640-9.

[4] Lee CS, Hegemier GA. Model of FRP-Confined Concrete Cylinders in Axial Compression. J Compos Constr. 2009;13(5):442-54.

[5] Teng JG, Jiang T, Lam L, Luo YZ. Refinement of a Design-Oriented Stress-Strain Model for FRP-Confined Concrete. J Compos Constr. 2009;13(4):269-78.

[6] Pham TM, Hadi MNS. Strain Estimation of CFRP Confined Concrete Columns Using Energy Approach. J Compos Constr. 2013;17(6):04013001.

[7] Ilki A, Peker O, Karamuk E, Demir C, Kumbasar N. FRP retrofit of low and medium strength circular and rectangular reinforced concrete columns. J Mater Civil Eng. 2008;20(2):169-88.

[8] Dai J-G, Bai Y-L, Teng JG. Behavior and modeling of concrete confined with FRP composites of large deformability. J Compos Constr. 2011;15(6):963-73.

[9] Ilki A, Kumbasar N, Koc V. Low strength concrete members externally confined with FRP sheets. Struct Eng Mechan. 2004;18(2):167-94.

[10] Rousakis TC, Karabinis AI. Adequately FRP confined reinforced concrete columns under axial compressive monotonic or cyclic loading. Mater Struct. 2012;45(7):957-75.

[11] Toutanji H, Han M, Gilbert J, Matthys S. Behavior of Large-Scale Rectangular Columns Confined with FRP Composites. J Compos Constr. 2010;14(1):62-71.

[12] Wang ZY, Wang DY, Smith ST, Lu DG. CFRP-Confined Square RC Columns. I: Experimental Investigation. J Compos Constr. 2012;16(2):150-60.

[13] Rousakis TC. Elastic fiber ropes of ultrahigh-extension capacity in strengthening of concrete through confinement. J Mater Civil Eng. 2014;26(1):34-44.

[14] Rousakis TC, Tourtouras IS. RC columns of square section - Passive and active confinement with composite ropes. Compos Part B-Eng. 2014;58:573-81.

[15] ACI 440.2R-08. Guide for the Design and Construction of Externally Bonded FRP Systems for Strengthening Concrete Structures. 4402R-08. Farmington Hills, MI: American Concrete Institute; 2008.

[16] TR 55. Design guidance for strengthening concrete structures using fibre composite materials. Camberley: Concrete Society; 2012.

[17] MacGregor JG. Reinforced concrete: mechanics and design. Upper Saddle River, N.J: Prentice Hall; 2005.

[18] Mander JB, Park R, Priestley MJN. Theoretical Stress-Strain Model for Confined Concrete. J Struct Eng. 1988;114(8):1804-26.

[19] Australian Standard-1545. Methods for the Calibration and Grading of Extenometers. 1545-1976. Homebush, NSW 21401976.

[20] Jiang T, Teng JG. Analysis-oriented stress-strain models for FRP-confined concrete. Eng Struct. 2007;29(11):2968-86.

[21] ASTM. Standard test method for tensile properties of fiber reinforced polymer matrix composites used for strengthening of civil structures. D7565:2010. West Conshohocken, PA2010.

[22] Lam L, Teng JG. Stress–strain model for FRP-confined concrete under cyclic axial compression. Eng Struct. 2009;31(2):308-21.

[23] Wang ZY, Wang DY, Smith ST, Lu DG. CFRP-Confined Square RC Columns. II: Cyclic Axial Compression Stress-Strain Model. J Compos Constr. 2012;16(2):161-70.

[24] Lam L, Teng JG. Design-oriented stress-strain model for FRP-confined concrete. Constr Build Mater. 2003;17(6-7):471-89.

[25] Sargin M, Ghosh SK, Handa VK. Effects of lateral reinforcement upon the strength and deformation properties of concrete. Mag Concr Res. 1971;23(Compendex):99-110.

[26] Bank LC. Progressive Failure and Ductility of FRP Composites for Construction: Review. J Compos Constr. 2013;17(3):406-19.

[27] Priestley MJN, Seible F, Calvi GM. Seismic design and retrofit of bridges. New York: Wiley; 1996.

[28] ACI 318-11. Building Code Requirements for Structural Concrete and Commentary. Farmington Hills, Michigan, USA: American Concrete Institute (ACI); 2011.

List of Figures

List of Tables

377 Table 1. Test matrix

ID	Unconfined concrete strength (MPa)	Target axial strain (%)	Actual axial strain (%)	Predicted lateral strain (%)	Actual lateral strain (%)	Predicted strength (MPa)	Actual strength (MPa)	No. of FRP layers
C2-0.6	52	0.6	0.62	0.46	0.44	69	70	2
C2-1.0	52	1.0	1.12	0.77	0.68	80	83	2
C2-1.2	52	1.2	1.33	0.91	0.94	84	89	2
C2-1.4	52	1.4	1.56	1.04	0.92	88	88	2
C2-1.9	52	1.9	1.99	1.25	1.40	95	97	2
C3-0.6	52	0.6	0.66	0.37	0.34	73	77	3
C3-1.0	52	1.0	1.02	0.62	0.67	87	90	3
C3-1.4	52	1.4	1.35	0.83	0.70	98	96	3
C3-1.9	52	1.9	1.87	1.05	1.08	109	106	3
C3-2.4	52	2.4	2.64	1.25	1.31	120	124	3

378

379 Table 2. Residual strength of tested specimens

ID	Residual strength (MPa)	Compared to f_c' (%)	Ordinate of intersection* (MPa)
C2-0.6	28	54	33
C2-1.0	17	33	18
C2-1.2	-	-	13
C2-1.4	9	17	8
C3-0.6	30	58	32
C3-1.0	23	44	20
C3-1.4	9	17	12
C3-1.7	9	17	-

380 * The intersection was made between the unload curve of the corresponding specimen and the
381 unconfined concrete curve.

Figure 1

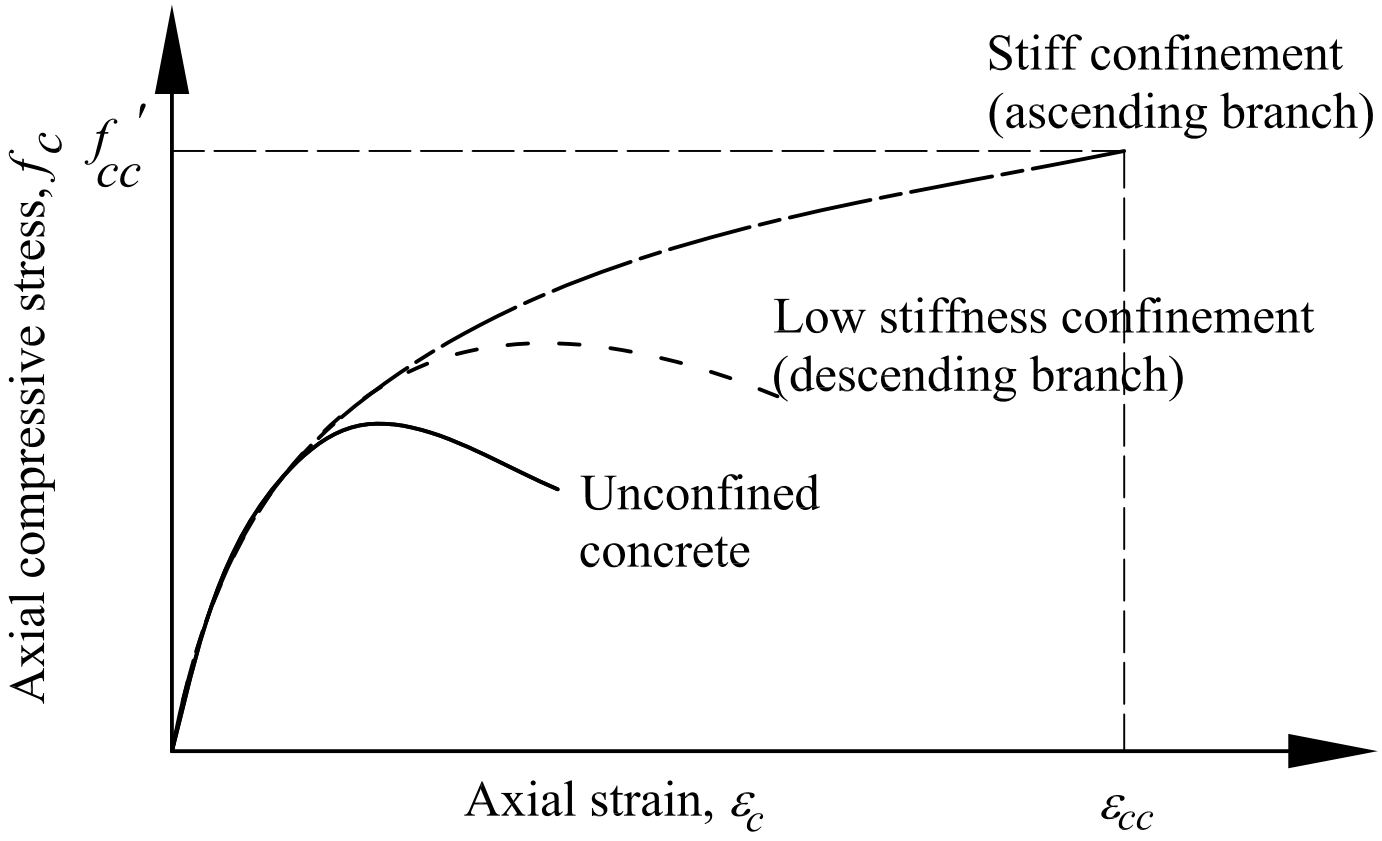
Stiff confinement
(ascending branch)
f_{cc}'
Low stiffness confinement
(descending branch)
Unconfined
concrete
Axial compressive stress, f_c
Axial strain, ε_c
ε_{cc}

Figure 2

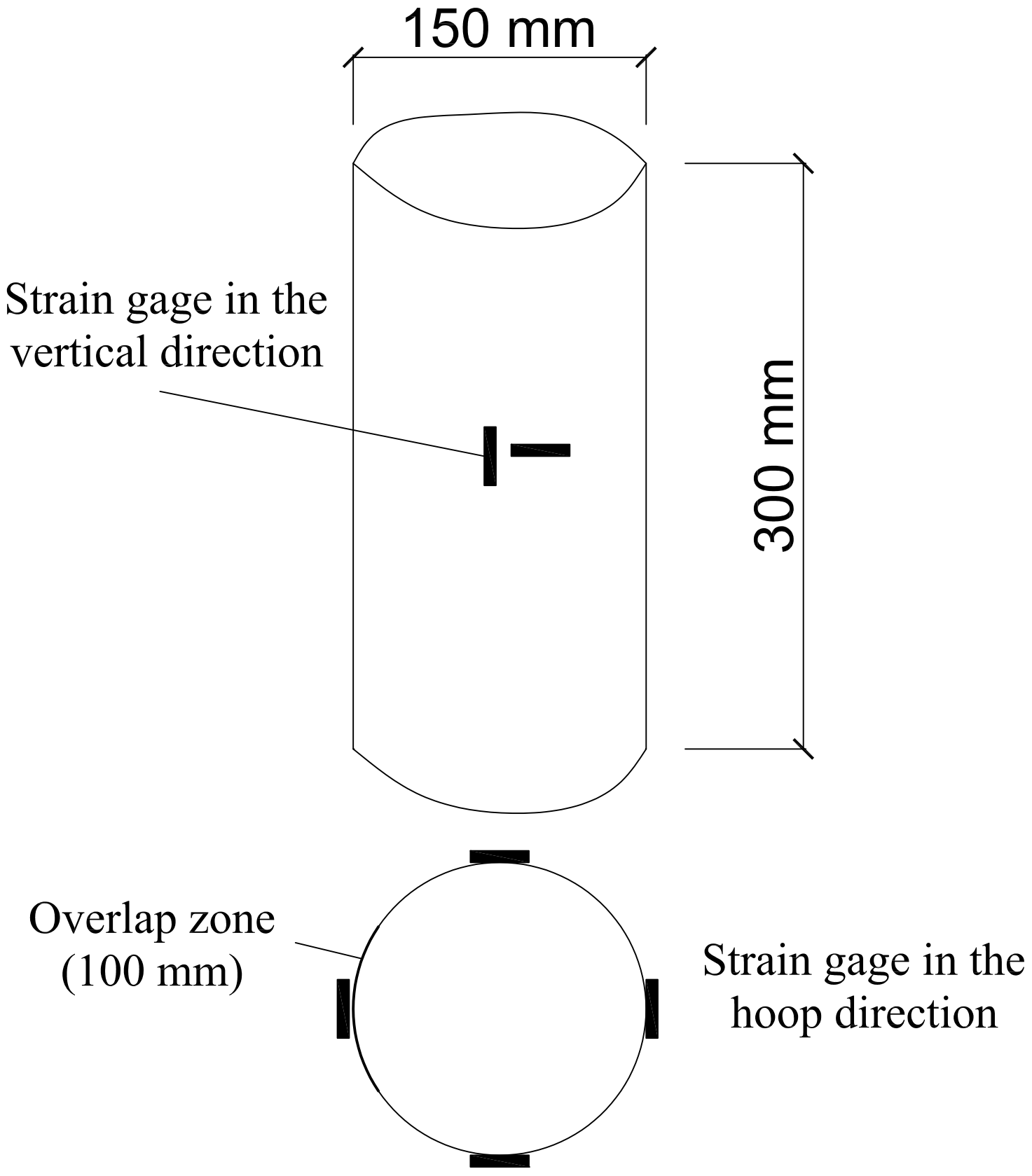
150 mm
Strain gage in the vertical direction
300 mm
Overlap zone (100 mm)
Strain gage in the hoop direction

Figure 3

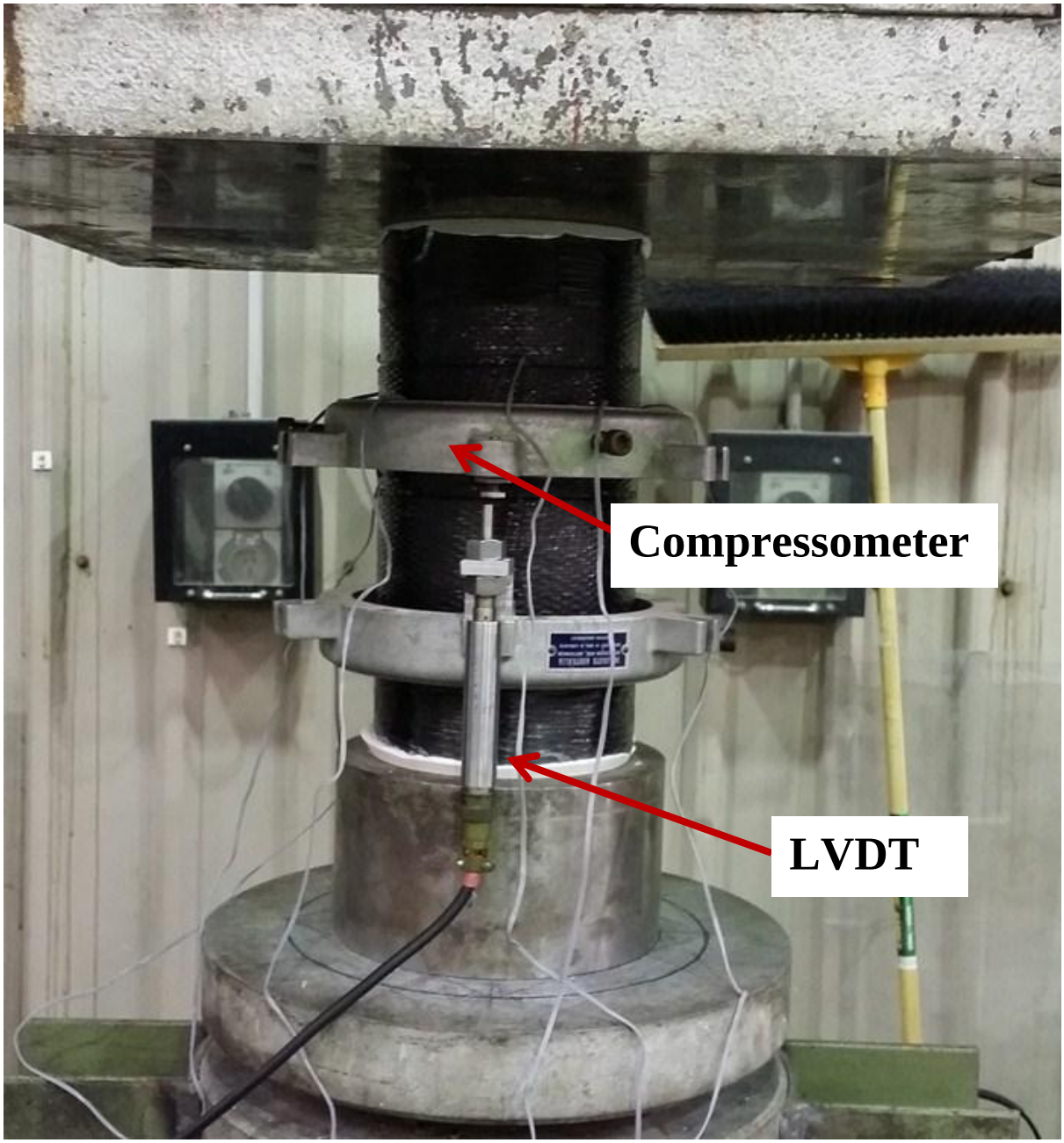

Figure 4

C2-1.2

C2-1.4

C3-1.4

C3-1.7

Figure 5

C2-0.6

C2-1.0

C3-0.6

C3-1.0

Figure 6

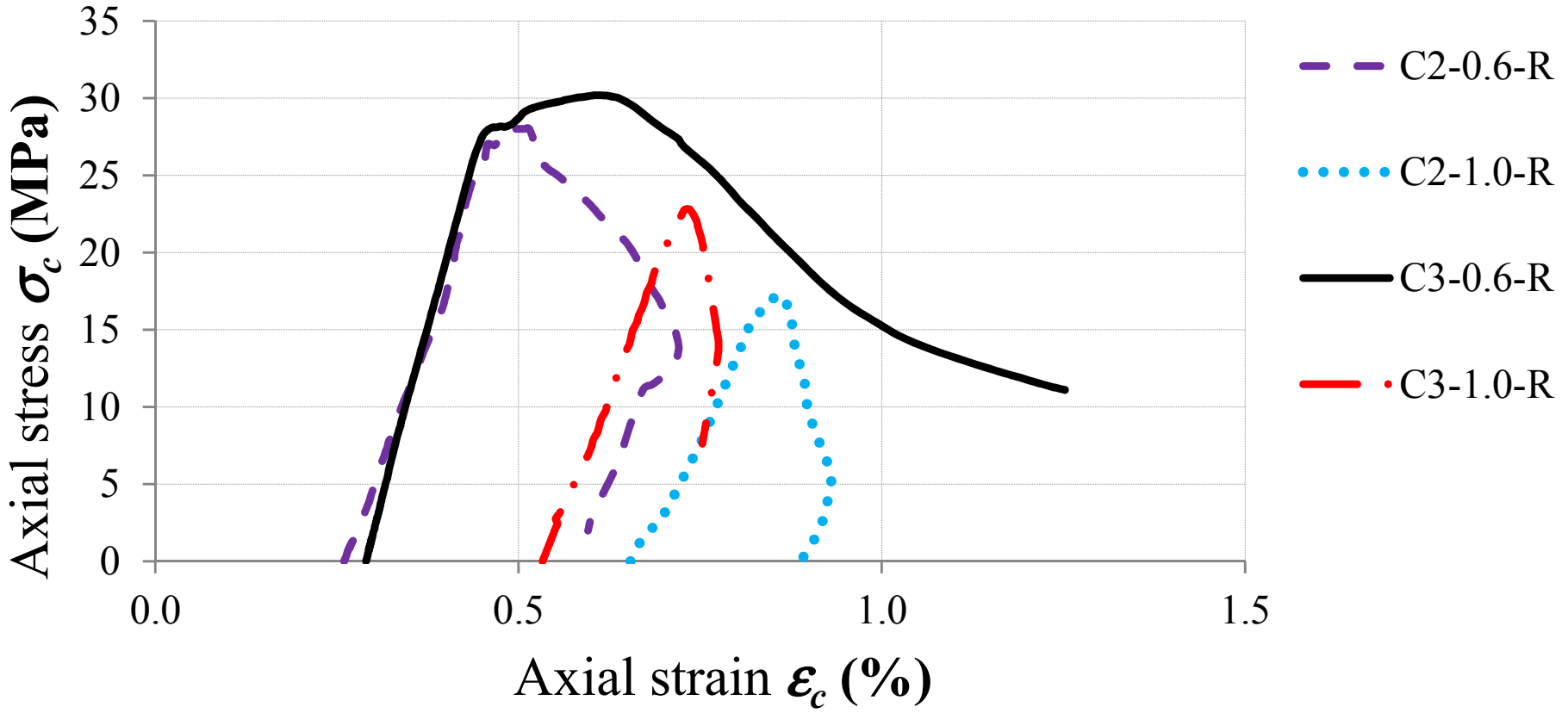
35
30
25
20
15
10
5
0
0.0
0.5
1.0
1.5
Axial stress σ_c (MPa)
Axial strain ε_c (%)
C2-0.6-R
C2-1.0-R
C3-0.6-R
C3-1.0-R

Figure 7

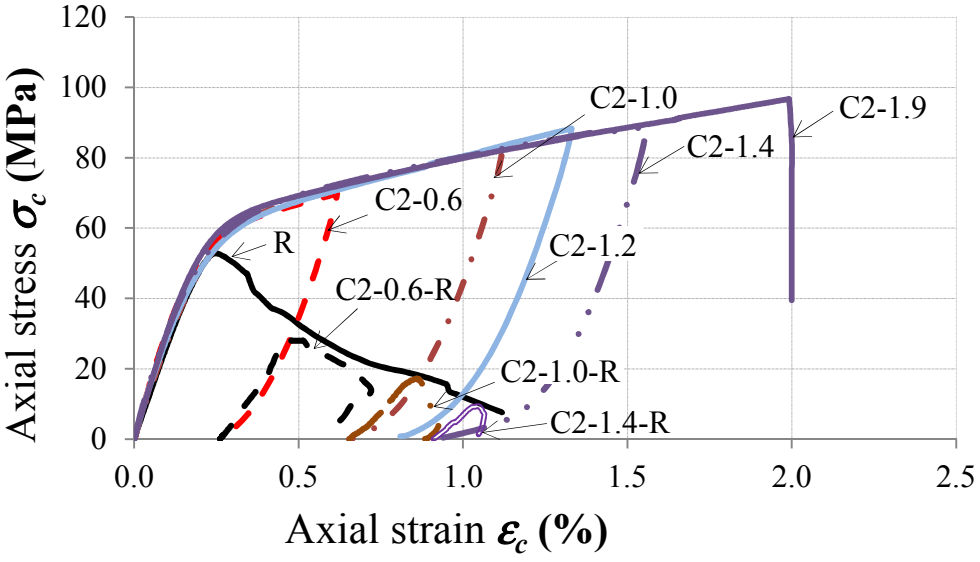
120
100
80
60
40
20
0
0.0
0.5
1.0
1.5
2.0
2.5
Axial stress σ_c (MPa)
Axial strain ε_c (%)
C2-1.0
C2-1.9
C2-1.4
C2-0.6
R
C2-1.2
C2-0.6-R
C2-1.0-R
C2-1.4-R

Figure 8

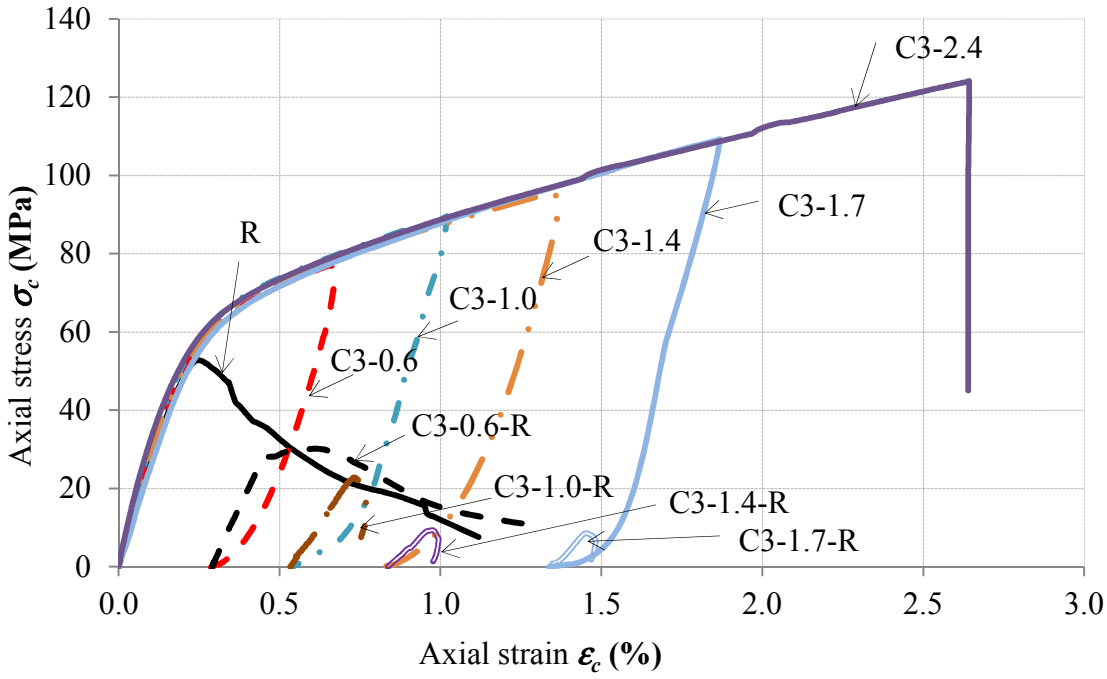
140
120
100
80
60
40
20
0
0.0
0.5
1.0
1.5
2.0
2.5
3.0
Axial stress σ_c (MPa)
Axial strain ε_c (%)
C3-2.4
C3-1.7
C3-1.4
C3-1.0
C3-0.6
R
C3-0.6-R
C3-1.0-R
C3-1.4-R
C3-1.7-R

Figure 9

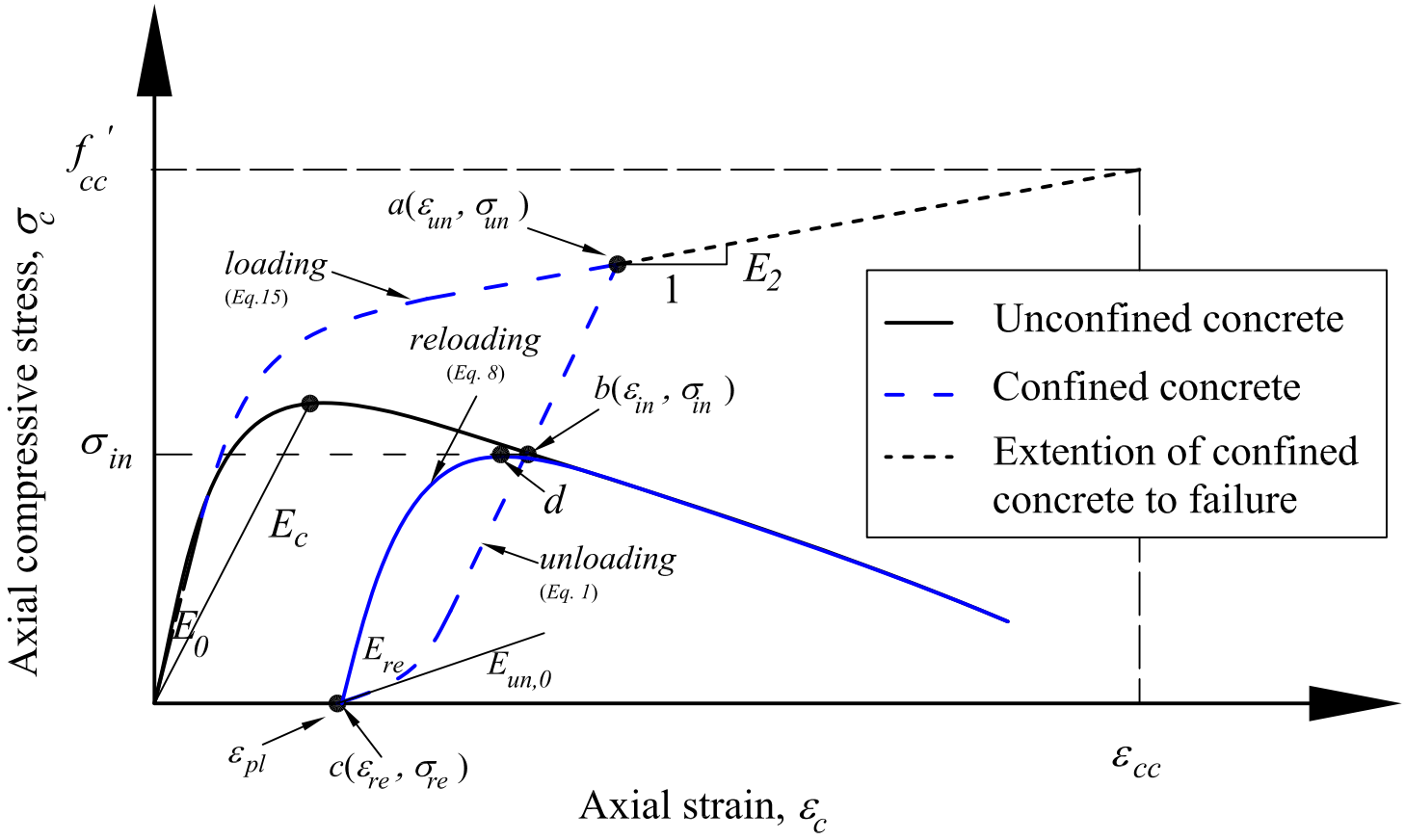
Axial compressive stress, σ_c
f'_{cc}
$a(\varepsilon_{un}, \sigma_{un})$
loading
(Eq.15)
1
E_2
reloading
(Eq. 8)
$b(\varepsilon_{in}, \sigma_{in})$
σ_{in}
E_c
d
unloading
(Eq. 1)
E_0
E_{re}
$E_{un,0}$
ε_{pl}
$c(\varepsilon_{re}, \sigma_{re})$
ε_{cc}
Axial strain, ε_c
Unconfined concrete
Confined concrete
Extention of confined concrete to failure

Figure 10

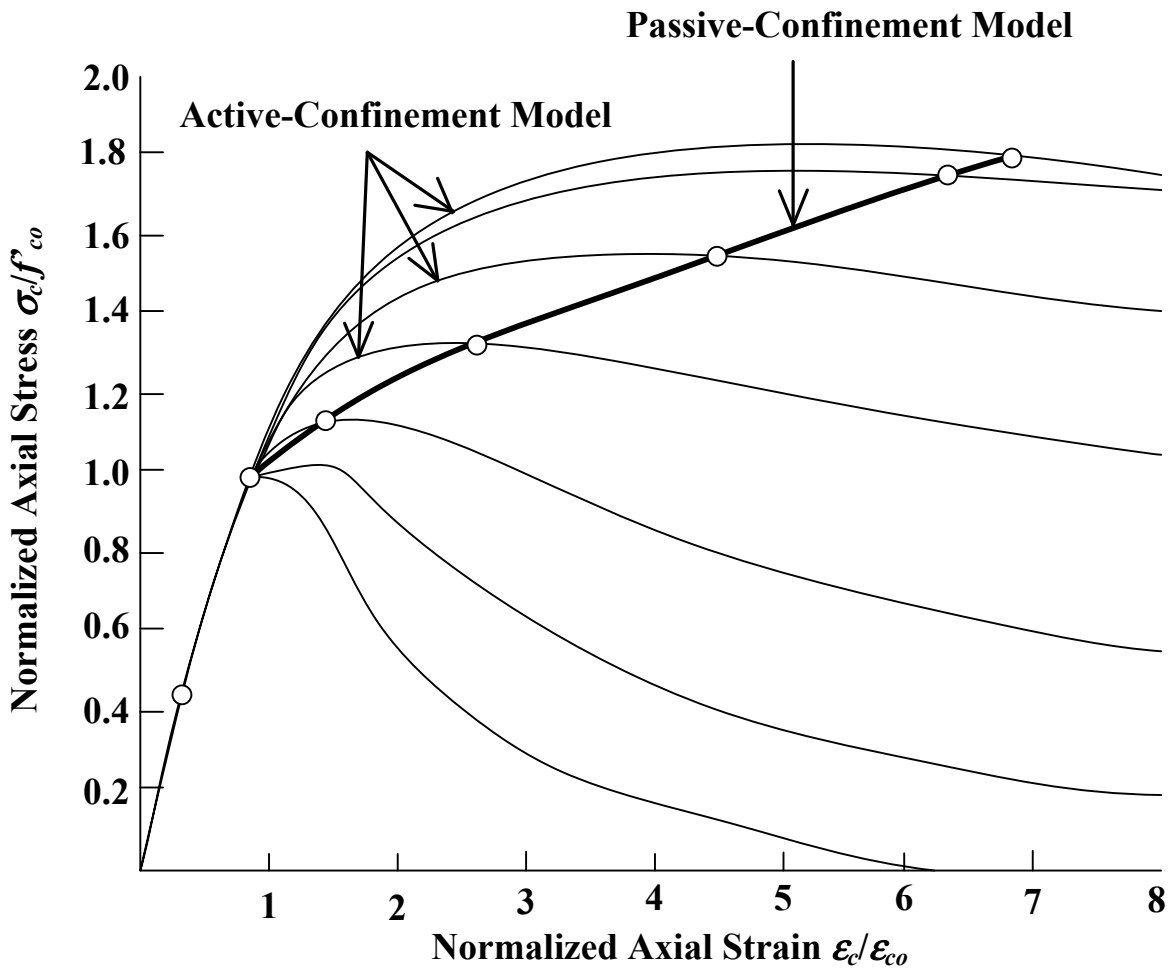
Passive-Confinement Model
Active-Confinement Model
Normalized Axial Stress σ_c/f'_{co}
Normalized Axial Strain $\varepsilon_c/\varepsilon_{co}$
2.0
1.8
1.6
1.4
1.2
1.0
0.8
0.6
0.4
0.2
1
2
3
4
5
6
7
8

Figure 11

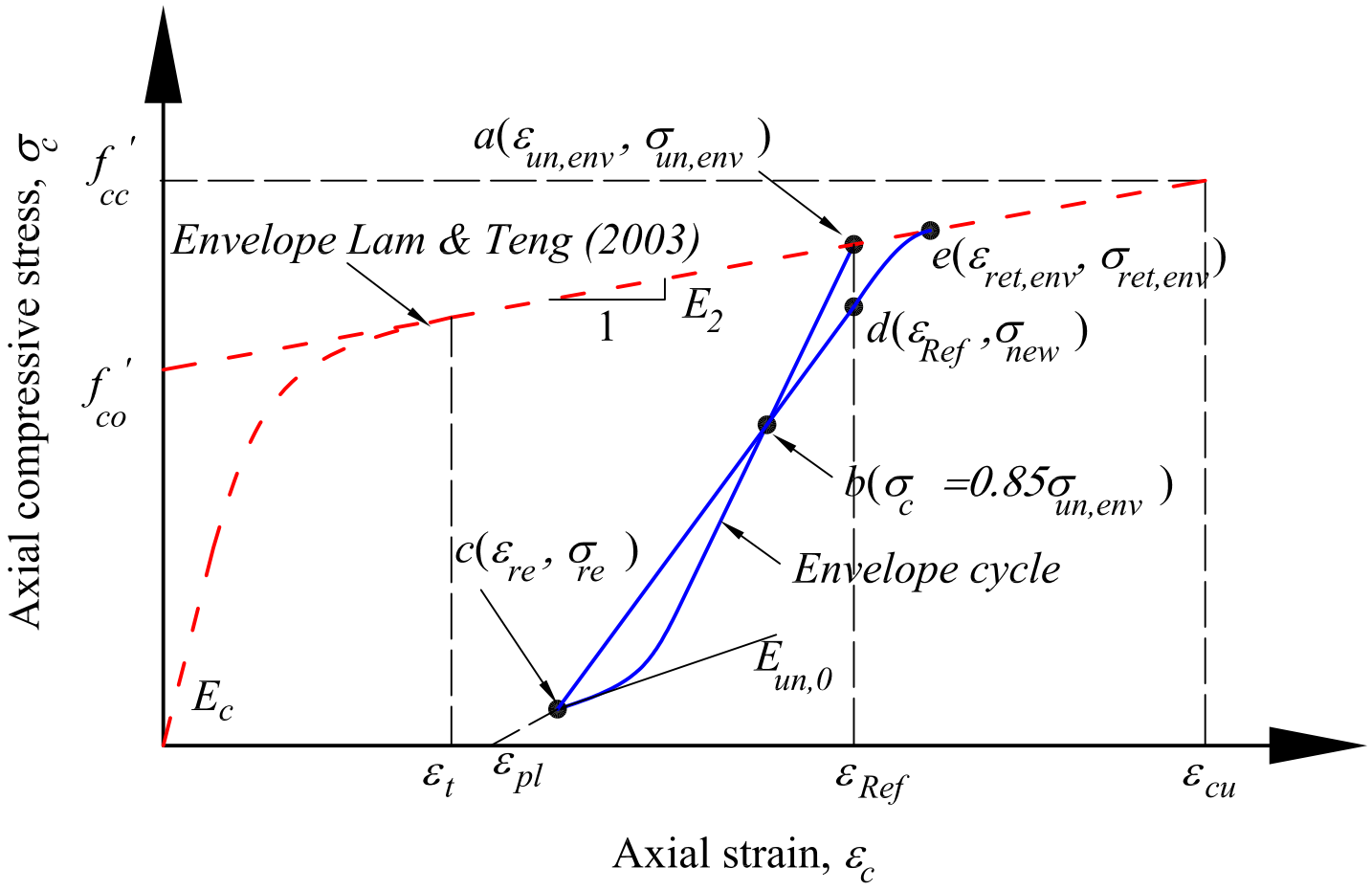
Axial compressive stress, σ_c
f_{cc}'
f_{co}'
$a(\varepsilon_{un,env}, \sigma_{un,env})$
Envelope Lam & Teng (2003)
1
E_2
$e(\varepsilon_{ret,env}, \sigma_{ret,env})$
$d(\varepsilon_{Ref}, \sigma_{new})$
$b(\sigma_c = 0.85\sigma_{un,env})$
$c(\varepsilon_{re}, \sigma_{re})$
Envelope cycle
$E_{un,0}$
E_c
ε_t
ε_{pl}
ε_{Ref}
ε_{cu}
Axial strain, ε_c

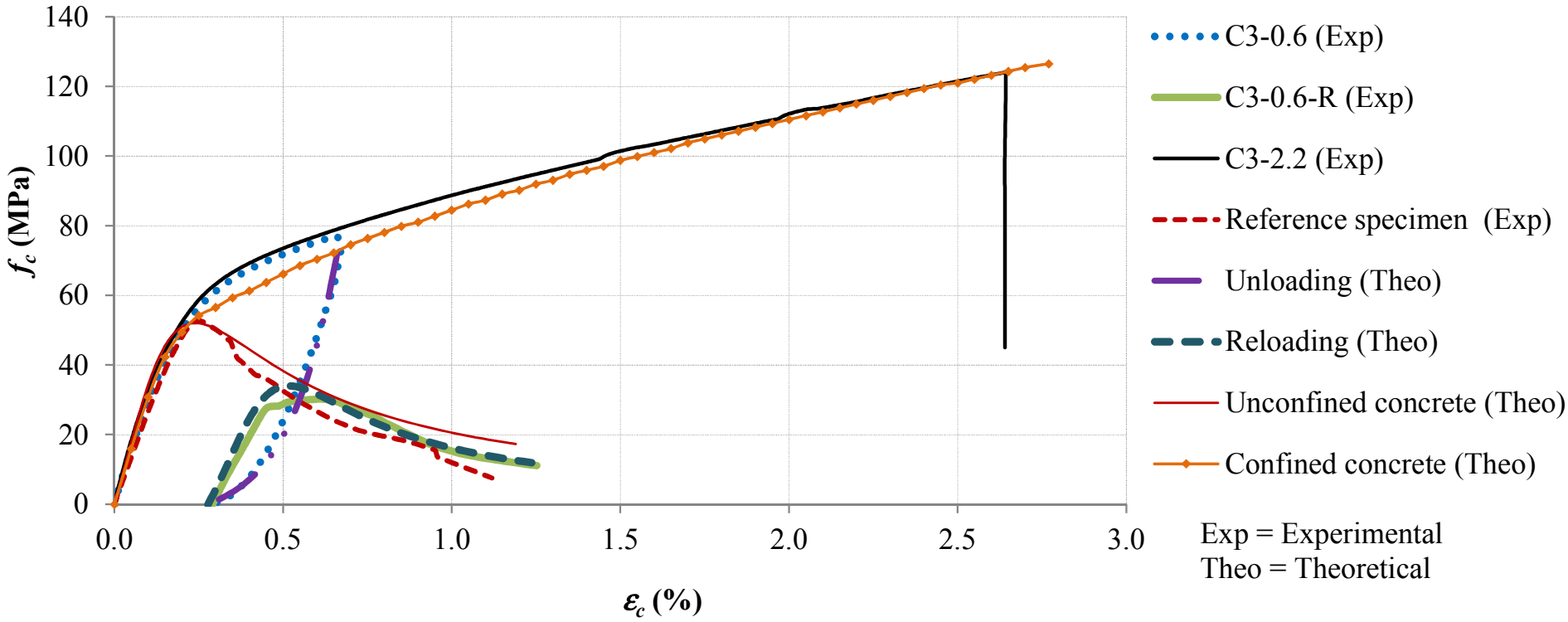
140
120
100
80
60
40
20
0
0.0
0.5
1.0
1.5
2.0
2.5
3.0
f_c (MPa)
ε_c (%)
C3-0.6 (Exp)
C3-0.6-R (Exp)
C3-2.2 (Exp)
Reference specimen (Exp)
Unloading (Theo)
Reloading (Theo)
Unconfined concrete (Theo)
Confined concrete (Theo)
Exp = Experimental
Theo = Theoretical

Figure 13

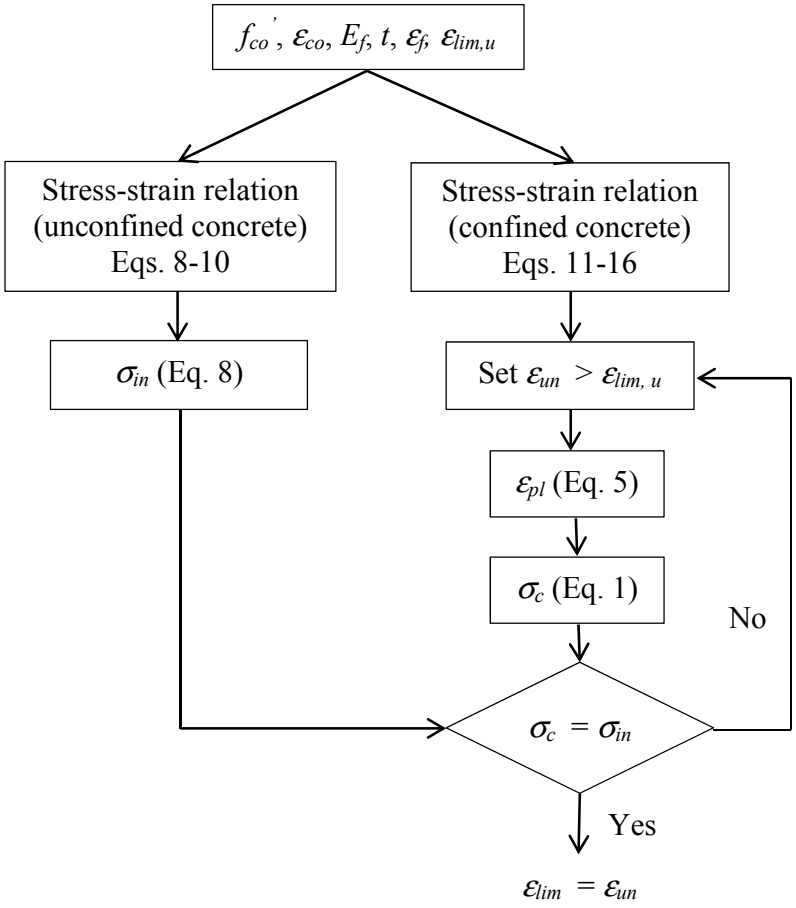
f_{co}', ε_{co}, E_f, t, ε_f, $\varepsilon_{lim,u}$
Stress-strain relation (unconfined concrete) Eqs. 8-10
Stress-strain relation (confined concrete) Eqs. 11-16
σ_{in} (Eq. 8)
Set $\varepsilon_{un} > \varepsilon_{lim,u}$
ε_{pl} (Eq. 5)
σ_c (Eq. 1)
No
$\sigma_c = \sigma_{in}$
Yes
$\varepsilon_{lim} = \varepsilon_{un}$